J Mater Sci: Mater Electron (2017) 28:14385–14393
DOI 10.1007/s10854-017-7299-2

Photoluminescence and photo-catalytic properties of $Zn_{1-x-y}Cu_xMn_yS$ nanostructures

Dinesh Kumar[1] · Ritika Monga[1] · I. S. Sandhu[2] · H. S. Bhatti[1] · Karamjit Singh[1]

Received: 27 January 2017 / Accepted: 5 June 2017 / Published online: 29 June 2017

Abstract $Zn_{1-x-y}Cu_xMn_yS$ $[(0 \le x \le 0.1), (0 \le y \le 0.1)]$ nanostructures have been synthesized by facile chemical co-precipitation technique at room temperature. Crystallographic, topographical and morphological characterization of synthesized nanomaterials have been done by X-ray diffraction, Scanning Electron Microscope and Transmission Electron Microscope, respectively. Synthesized nanoparticles crystallizes in zinc blende structure having average crystallite size nearly 2–3 nm. Comparison of the diffraction and electron microscopy studies reveal the formation of single nanocrystals. The energy dispersive X-ray spectroscopy and Fourier transform infrared spectroscopic studies have been carried for the detailed quantitative and qualitative analysis of synthesized nanostructures. Optical characterization of synthesized nanomaterials has been done by UV–visible absorption and steady state photoluminescence spectroscopic studies. The room temperature energy resolved photoluminescence (PL) spectra show multi-chromatic emissions originating from the host and dopant related defect states. The photo-catalytic activity of synthesized nanomaterials under UV irradiation have been tested using methylene blue (MB) dye as test contaminant in aqueous media. Photo-physical and photo-chemical behaviour dependence on doping concentration has been thoroughly studied to explore the potential of synthesized nanomaterials for next era opto-electronic industrial applications as well as polluted water purification.

✉ Karamjit Singh
dhaliwalkaramjit@gmail.com

[1] Department of Physics, Punjabi University, Patiala 147 002, Punjab, India

[2] Department of Applied Sciences, Chitkara University, Rajpura 140401, Punjab, India

1 Introduction

Semiconducting nanocrystalline materials have attracted tremendous attention in electronics and photonics [1]. Semiconductor nanocrystals are described as a state of matter, which is intermediate between individual molecules and bulk materials. Transition from bulk materials to nanoparticles lead to the display of quantum mechanical properties and an increased dominance of surface atoms, which increases the chemical reactivity of a material [2]. Notable examples of change in physical and chemical properties mainly include tunable bandgap [3] and catalytic behaviour [4]. The small size and high optical activity of certain semiconductors make them interesting for applications in disciplines ranging from opto-electronics [4], catalysis [5] to fluorescence microscopy [6].

Semiconductor nanocrystals are potentially useful for technological applications like indicators [7], analysis of water pollution, environmental studies, pathological investigations etc. The change in the properties of nanoparticles is driven mainly by two factors, namely the increase in the surface to volume ratio and change in the electronic structure of the material due to quantum confinement effects [8]. Particles in nanometric sizes show unique physical and chemical properties, for example with the decrease of particle size, extremely high surface area to volume ratio is obtained leading to an increase in surface specific active sites for chemical reactions and photon absorption to enhance the reaction and absorption efficiency [9]. The enhanced surface area to volume ratio increases surface states, which changes the activity of electrons and holes, affecting the chemical reaction dynamics. Since nanostructures have large surface to volume ratio, and interface effects resulting novel phenomena. Therefore, nanobuilding materials such as ZnO nanowires, carbon nanotubes, ZnS

nanoparticles, CdSe nanoparticles, GaN nanowires etc. are intensively investigated for their potential applications.

ZnS is one of the first discovered II–VI compound semiconductor materials with versatile fundamental properties [10]. Due to its wide band-gap of ~3.7 eV, ZnS is widely used as phosphor and heterogeneous photo-catalyst [11–13]. ZnS nanoparticles have attracted great interest of researchers due to their excellent size tunable optical properties. It has been reported that doping in ZnS nanoparticles enhances the optical transition efficiencies of carriers, and increases the number of optically active sites [14, 15]. Novel luminescence characteristics, such as stable, fast and intense visible light emission with different colours have been observed from doped ZnS nanocrystals [16, 17].

In the present study, polyvinyl alcohol (PVA) capped pure and doubly doped (dopants: Mn and Cu) ZnS nanocrystals have been synthesized by chemical co-precipitation method. The effect of doping concentration on crystallography, morphology, photoluminescence and photo-catalytic activity of synthesized nanocrystals has been thoroughly studied. To the best of our knowledge, present paper is the first report mentioning the photo-catalytic activity of $Zn_{1-x-y}Cu_xMn_yS$ $[(0 \le x \le 0.1), (0 \le y \le 0.1)]$ nanocrystals.

2 Experimental

Polyvinyl alcohol (PVA) capped $Zn_{1-x-y}Cu_xMn_yS$ $[(0 \le x \le 0.1), (0 \le y \le 0.1)]$ nanocrystals have been synthesized in aqueous media under ambient conditions using chemical co-precipitation method already described by Singh et al. [18]. Analytical reagent grade chemicals: Zinc acetate ($C_4H_6O_4Zn{\cdot}2H_2O$), Cupric Chloride ($CuCl_2$), Manganese Chloride ($MnCl_2$), Sodium Sulphide ($Na_2S{\cdot}xH_2O$) and PVA $(C_2H_4O)_n$ procured from Hi Media laboratories Pvt. Ltd. Mumbai (India) and S. D. Fine-Chem Ltd. Mumbai (India) were used without further purification. The aqueous solutions of all the precursors were mixed in stoichiometric concentrations under vigorous stirring. In addition, 2% PVA solution was added to reaction media to avoid the agglomeration. The resulting precipitates were filtered and vacuum dried at 80 °C for 16 h.

Crystallographic analyses of the synthesized nanomaterials were done using Rigaku Miniflex-600 powder X-ray diffractometer (XRD). XRD patterns of all the synthesized samples were recorded with Cu Kα radiation (λ = 1.54 Å) keeping step size 0.02° at scan speed of 4.00°/min in 2θ range 20°–70° at generator tension 40 kV and generator current 15 mA. Electron micrographs were recorded using JEOL JSM-6510LV SEM operating at 10–15 keV for topographical studies, whereas Hitachi H-7500 TEM operating at 100 keV has been used for morphological studies. For the quantitative and qualitative analyses, EDS and FTIR spectra were recorded using Zeiss Supra 55 Oxford Instruments FESEM equipped with EDS and Perkin Elmer Spectrum-400 FTIR spectrometer, respectively.

Hitachi U-2900 UV–Vis absorption spectrophotometer and Perkin Elmer LS 55 Fluorescence spectrometer were used to record the room temperature absorption and emission spectra of synthesized nanostructures dissolved in dimethylformamide (DMF).

The photocatalytic activity of synthesized nanocrystals was examined by monitoring the degradation of MB dye in aqueous media under UV radiation exposure. Dye contaminated aqueous media was prepared by dissolving 0.001 g of MB dye in 1000 ml of distilled water. Then 0.080 g of nanophotocatalyst was dispersed in dye contaminated aqueous media, the resulting aqueous suspension was equilibrated by stirring in dark for 80 min. Then, the aqueous suspension was irradiated with UV radiations (λ = 200–400 nm) for 80 min. During the irradiation process, after every 10 min. the sample was collected. Absorption spectra of all the collected samples were recorded to calculate the remnant dye concentration.

3 Results and discussions

Aqueous chemical co-precipitation method is a facile eco-friendly bottom-up synthesis technique which gives good yield of $Zn_{1-x-y}Cu_xMn_yS$ $[(0 \le x \le 0.1), (0 \le y \le 0.1)]$ nanostructures. Figure 1 shows the XRD patterns recorded for ZnS and $Zn_{0.80000}Cu_{0.10000}Mn_{0.10000}S$ prepared by chemical co-precipitation method. It can be clearly seen from the recorded diffractograms that all the recorded XRD patterns show peak broadening due to nanosize formation. Comparison of the recorded XRD patterns with standard JCPDS data base (JCPDS card no. 77-2100) reveals that the synthesized materials are zinc blende structured ZnS nanocrystals. No impurity phase has been observed in the recorded diffractograms. The average crystallite size values calculated using Scherrer formula [19, 20] from recorded diffractograms are ~2–3 nm.

Figures 2 and 3 show SEM micrographs recorded for ZnS and $Zn_{0.80000}Cu_{0.10000}Mn_{0.10000}S$ nanocrystals, respectively. The recorded backscattered and secondary electron micrographs show the formation of nearly smooth surfaced agglomerates of micrometer dimensions. SEM was unable to measure the morphology of synthesized nanocrystals as these have ultra small sizes on nanoscale which is beyond the detection range of conventional SEM operating at accelerating voltages ~10–15 keV.

The EDS spectra recorded for ZnS and $Zn_{0.80000}Cu_{0.10000}Mn_{0.10000}S$ nanocrystals are shown in Fig. 4. Spectrum 1 in Fig. 4 reveals the formation of

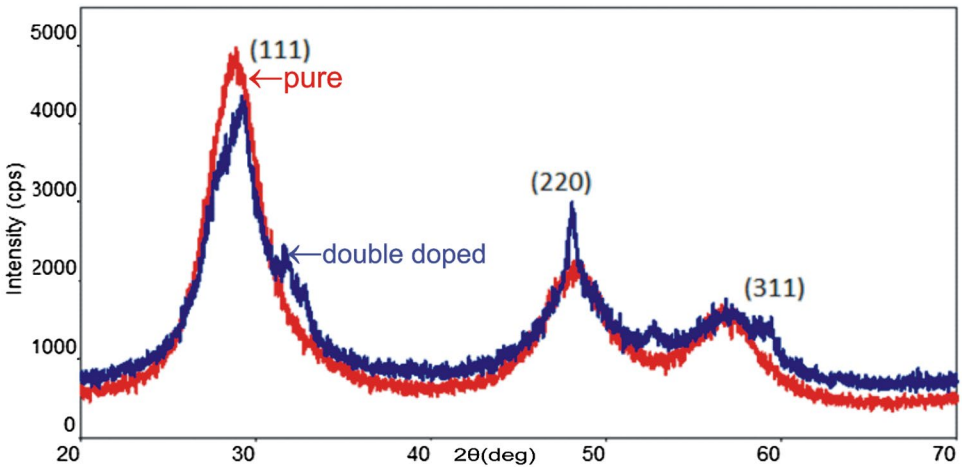

Fig. 1 XRD patterns of ZnS and $Zn_{0.80000}Cu_{0.10000}Mn_{0.10000}S$ nanocrystals

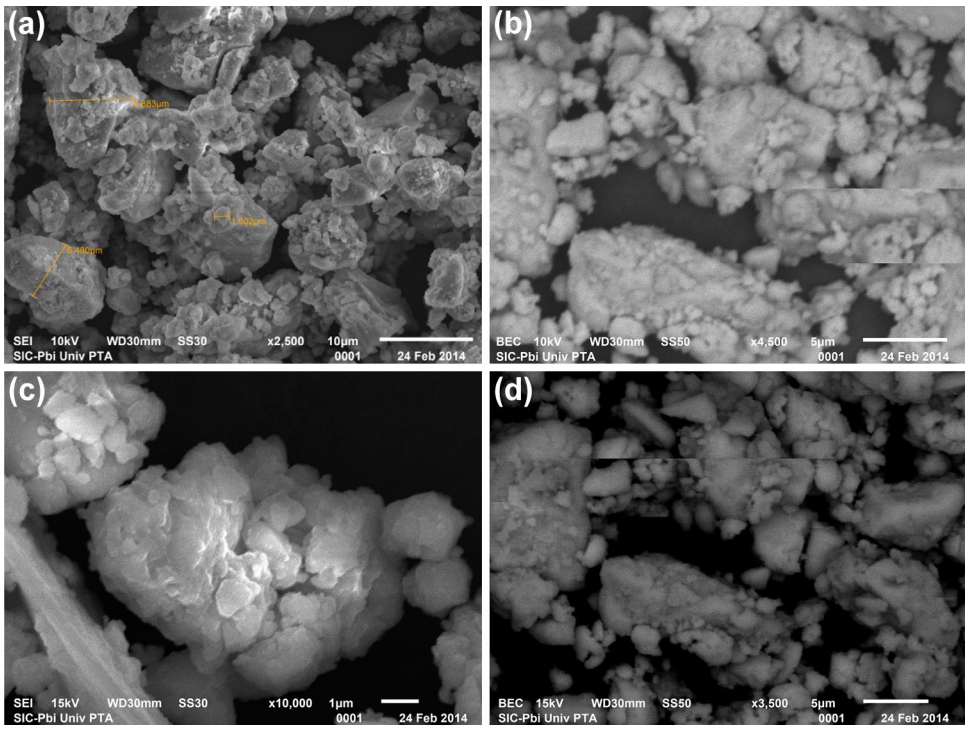

Fig. 2 SEM micrographs of ZnS nanoparticles

intrinsic ZnS without presence of any impurity. The X-ray peaks indicate 48.98 wt% (19.03 at.%) and 15.59 wt% (12.35 at.%) content of zinc and sulphur, respectively. Carbon [23.52 wt% (49.72 at.%)] and oxygen [11.91 wt% (18.90 at.%)] are also present along with zinc and sulphur which confirm the presence of PVA capping layer.

Spectrum 2 in Fig. 4 recorded for $Zn_{0.80000}Cu_{0.10000}Mn_{0.10000}S$ nanocrystals show 42.40 wt% (16.97 at.%), 6.61 wt% (2.72 at.%), 16.07 wt% (13.11 at.%) and 0.55 wt% (0.41 at.%) content of zinc, copper, sulphur and chlorine, respectively. Presence of chlorine may reduce the manganese, this may be the reason for the absence of manganese peak in the recorded EDS spectra. Moreover, X-ray peaks corresponding to carbon [19.53 wt% (42.55 at.%)] and oxygen [14.83 wt% (24.24 at.%)] are also present due to PVA capping layer.

Figures 5 and 6 show TEM micrographs recorded for ZnS and $Zn_{0.80000}Cu_{0.10000}Mn_{0.10000}S$ nanoparticles, respectively. The electron micrographs are obtained at 100 keV accelerating voltage at variable magnifications [$(2–5)\times10^5\times$]. The average particle size values calculated from TEM micrographs were ~2–3 nm. Comparison of XRD and TEM results reveal that the synthesized nanoparticles are single nanocrystals.

Figure 7 shows the FTIR spectra recorded for ZnS and $Zn_{0.80000}Cu_{0.10000}Mn_{0.10000}S$ nanocrystals. All the

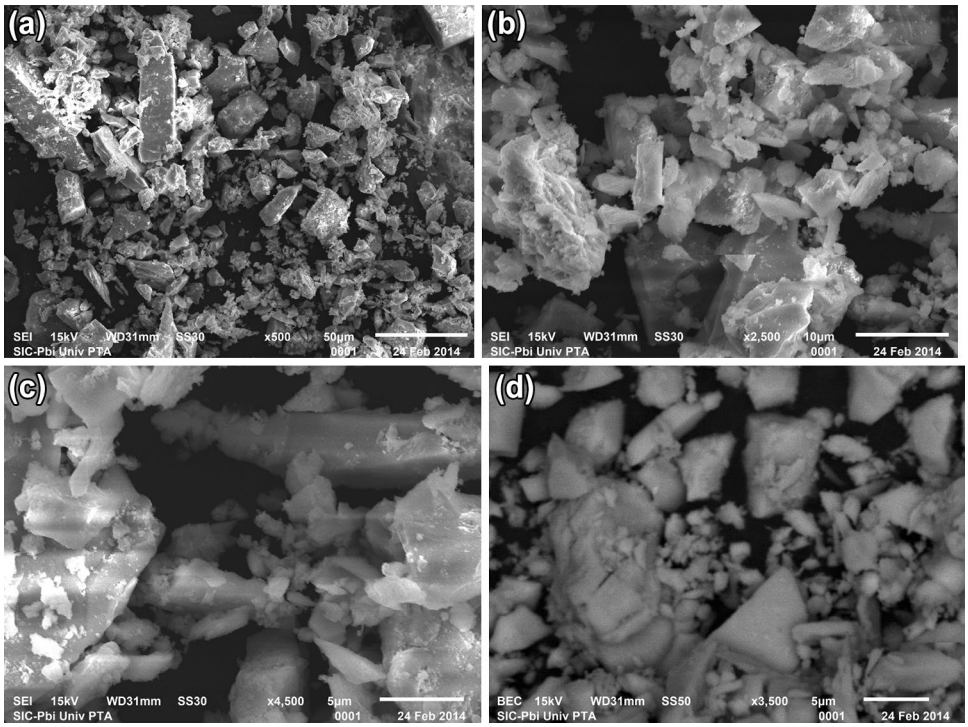

Fig. 3 SEM micrographs of $Zn_{0.80000}Cu_{0.10000}Mn_{0.10000}S$ nanoparticle

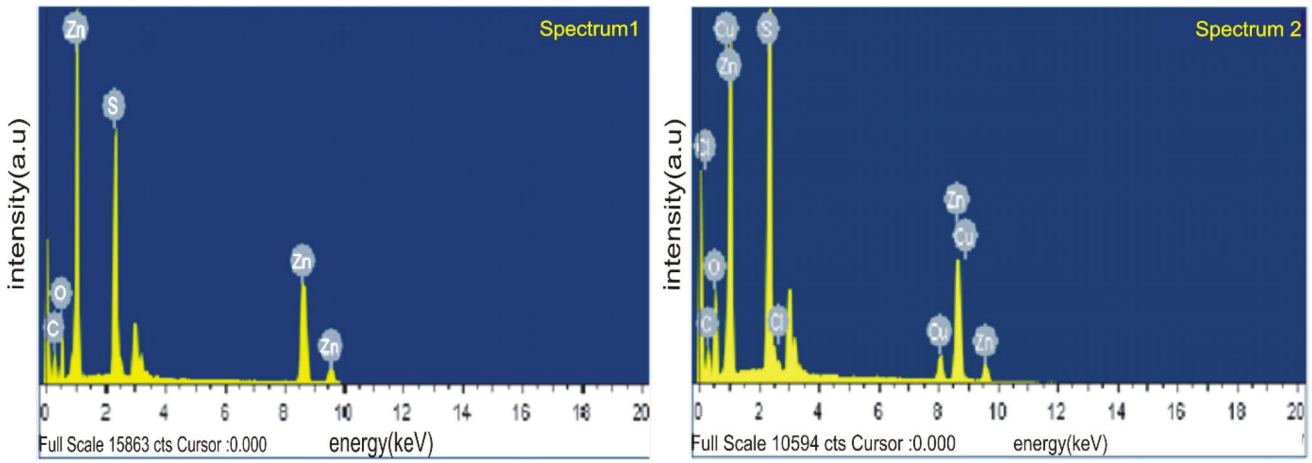

Fig. 4 EDS spectra of ZnS (*Spectrum 1*) and $Zn_{0.80000}Cu_{0.10000}Mn_{0.10000}S$ nanocrystals (*Spectrum 2*)

FTIR spectra were recorded in the range 4000–400 cm^{-1}. Recorded spectra infer that peak at 3398 cm^{-1} is ascribed to the O–H stretching of water molecules or PVA. The peaks at 1556–58 and 1115–1020 cm^{-1} are due to stretching and bending of C=C bonds, whereas 1400–06 and 1338–41 cm^{-1} peaks are due to C–H and C–H_2 bending and stretching modes. The peaks appeared at 671 and 616 cm^{-1} reveal the formation of Zn–S bond.

The FTIR spectra of pure and doubly doped ZnS nanocrystals are approximately same governs for no other formation of contaminated bonds due to doping. On the otherhand, it can be clearly seen from the recorded spectra that the addition of dopants causes decrease in transmission intensity followed by slight augmentation of broadness of peaks. This is believed to be due to the presence of the additional metal bonds caused by double doping in ZnS. Thus, FTIR studies strongly support the formation of PVA encapsulated pure and doubly doped ZnS nanocrystals.

Figure 8 shows UV–Vis absorption spectra recorded for $Zn_{1-x-y}Cu_xMn_yS$ [$(0 \le x \le 0.1)$, $(0 \le y \le 0.1)$] nanocrystals. It can be clearly seen from the recorded spectra that synthesized nanocrystals have broad absorption profiles.

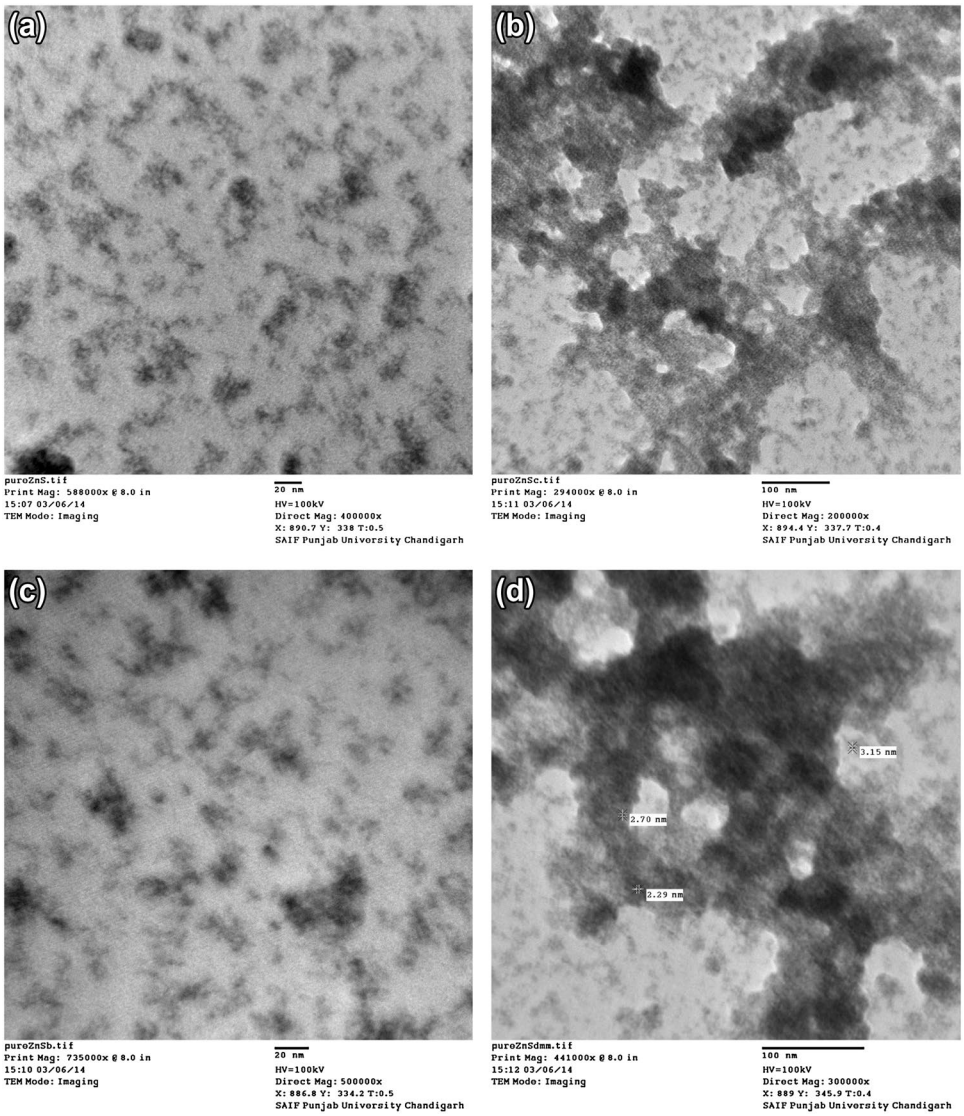

Fig. 5 TEM micrographs of ZnS nanoparticles

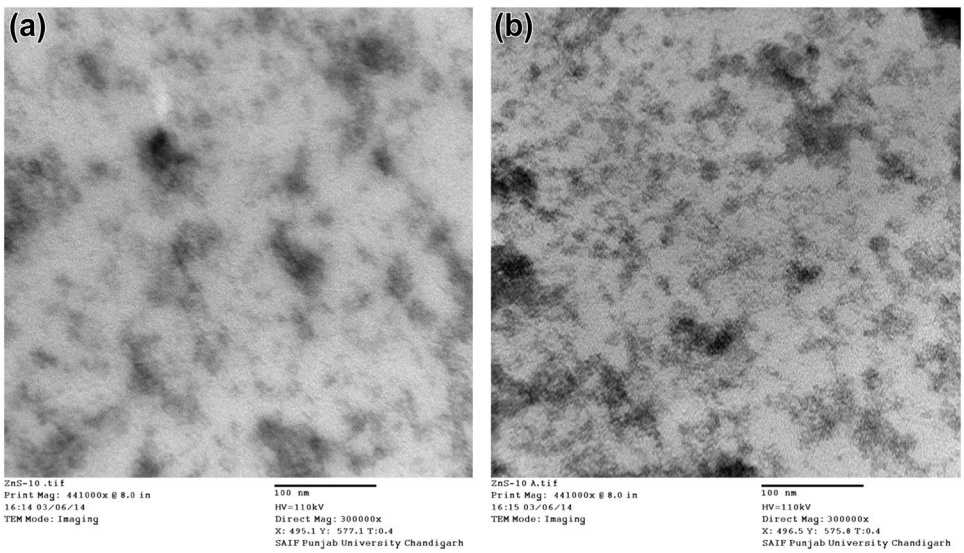

Fig. 6 TEM micrographs of $Zn_{0.80000}Cu_{0.10000}Mn_{0.10000}S$ nanoparticles

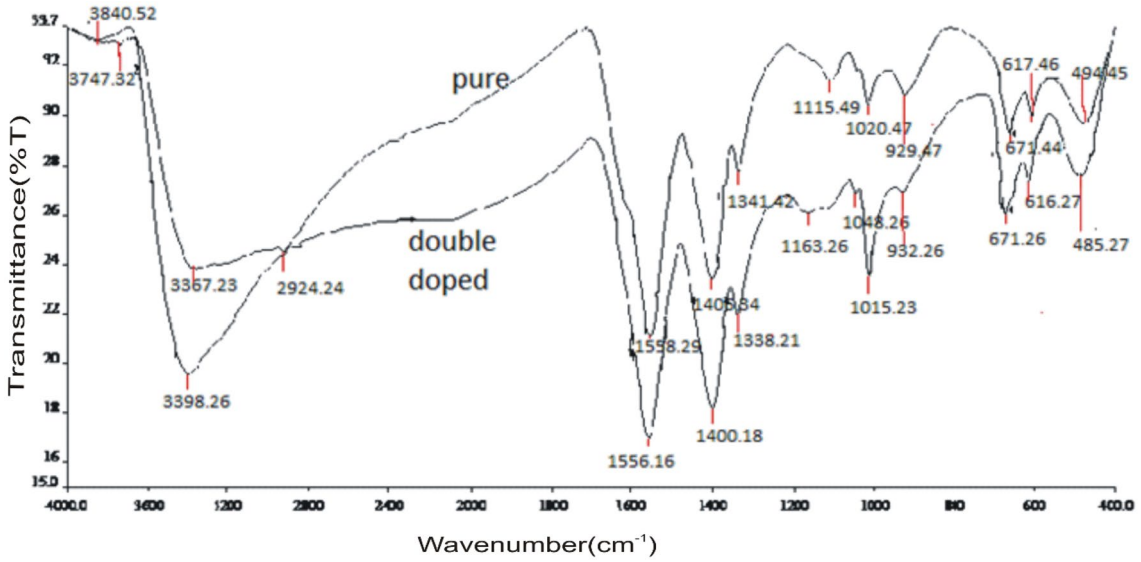

Fig. 7 FTIR spectra of ZnS and $Zn_{0.80000}Cu_{0.10000}Mn_{0.10000}S$ nanocrystals

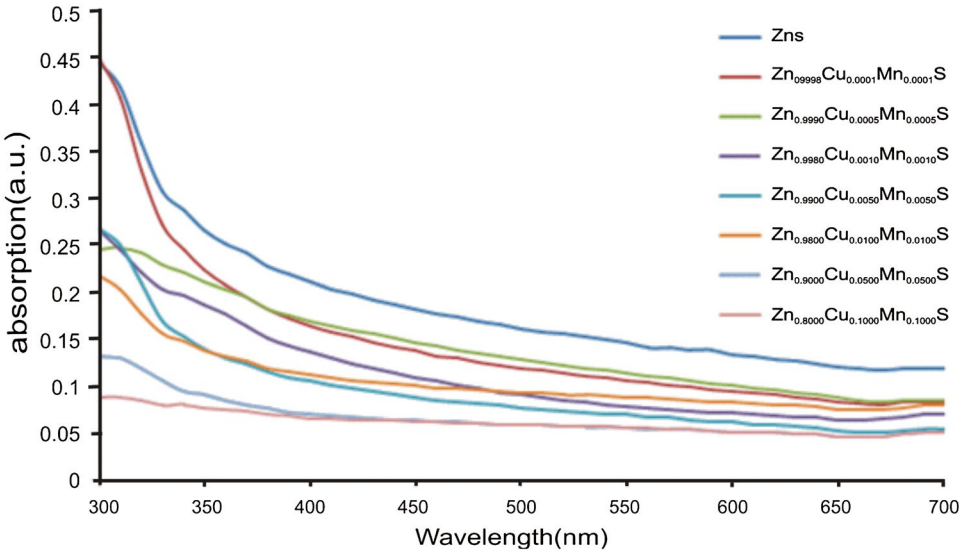

Fig. 8 Absorption spectra of $Zn_{1-x-y}Cu_xMn_yS$ nanocrystals

Absorption edges slightly shifts towards the blue with the addition of dopants in the host lattice. This may be due to the band gap broadening caused by quantum confinement effect. As, dopant ions (Mn^{2+} and Cu^{2+}) have smaller ionic radii w.r.t. Zn^{2+} ions, so the replacement of Zn^{2+} ions by dopants may cause the shrinkage of crystallite/particle size, which effects the electronic structure of the host lattice.

Figure 9 shows the room temperature energy resolved photoluminescence spectra of synthesized nanocrystals excited at 325 nm. Pure ZnS nanocrystals give broad violet blue emission ($\lambda_{Max.Intensity}$ ~400 nm) originating from host related defect states. Doubly doped ZnS nanocrystals show multi-chromatic emission spectra (λ_{peak} ~400–435 nm, λ_{peak} ~530–535 nm and λ_{peak} ~580 nm) along with shoulder at ~370–375 nm. Ultraviolet and violet blue emissions may originate from the shallow and deep host related trapping states. The orange emission (λ_{peak} ~580 nm) corresponds to the $^4T_1 \rightarrow {}^6A_1$ transitions of Mn^{2+} dopant ions. The addition of dopants in $Zn_{1-x-y}Cu_xMn_yS$ nanocrystals beyond minimum critical concentration ($x = y = 0.0005$) also show feeble green emission (λ_{peak} ~530–535 nm) which occurs due to $^2T_2 \rightarrow {}^2E_1$ transitions of Cu^{2+} ions substituted in tetrahedral sites. Crystal field of tetrahedral symmetry split Cu^{2+} ground state into $^2T_2$ and ^2E levels. It can be clearly seen from the recorded PL spectra that the intensity of host related radiative transitions diminishes with the increasing

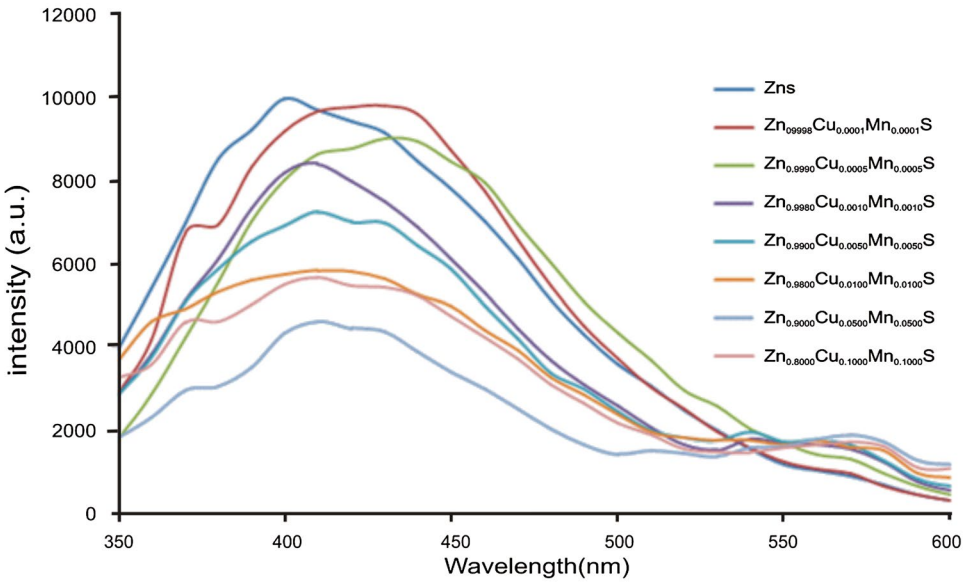

Fig. 9 PL spectra of $Zn_{1-x-y}Cu_xMn_yS$ nanocrystals

concentration of dopant defect states whereas dopant related PL peaks intensity go on increasing with increasing concentration of dopants.

Figure 10 shows the absorption spectra of MB dye solution at different time intervals of UV radiation exposure in the presence of ZnS nanocrystals. It can be clearly seen from the Fig. 10 that ZnS nanocrystals behave as efficient nano-photocatalyst. There is a concentration dependent slight spectral shift in MB dye absorption spectra as the UV irradiation time changes from 0 to 60 min. Blue shift in the absorption peak with decreasing dye concentration has been observed due to diminished optical density.

Figure 11 shows the $Zn_{1-x-y}Cu_xMn_yS$ $[(0 \le x \le 0.1), (0 \le y \le 0.1)]$ nanocrystals sensitized photo-degradation of MB dye under UV radiations exposure. Figure 11 clearly indicates that MB dye is degraded to maximum extent in case of $Zn_{0.80000}Cu_{0.10000}Mn_{0.10000}S$ nanocrystals, whereas ZnS or slightly doubly doped ZnS nanocrystals degrade MB dye to minimum extent. Beyond the optimum doping concentration $(x = y = 0.005)$ photo-catalytic activity of $Zn_{1-x-y}Cu_xMn_yS$ nanocrystals drastically enhances with augmentation of doping concentration. This augmentation of photo-catalytic activity is caused by the increased interfacial charge transfer at higher doping concentrations. Moreover, addition of dopants may lengthen the excited state life of charge carriers, which results the enhanced photo-catalytic activity.

Comparison of PL and photo-catalytic activity results reveal that the competition between the charge carrier recombination and charge carrier trapping followed by the competition between recombination of trapped carriers and interfacial charge transfer determine the overall quantum efficiency for interfacial charge transfer. This is the reason that the host related PL emission intensity go on decreasing with addition of dopants, whereas photo-catalytic activity enhances by many folds at higher doping concentrations.

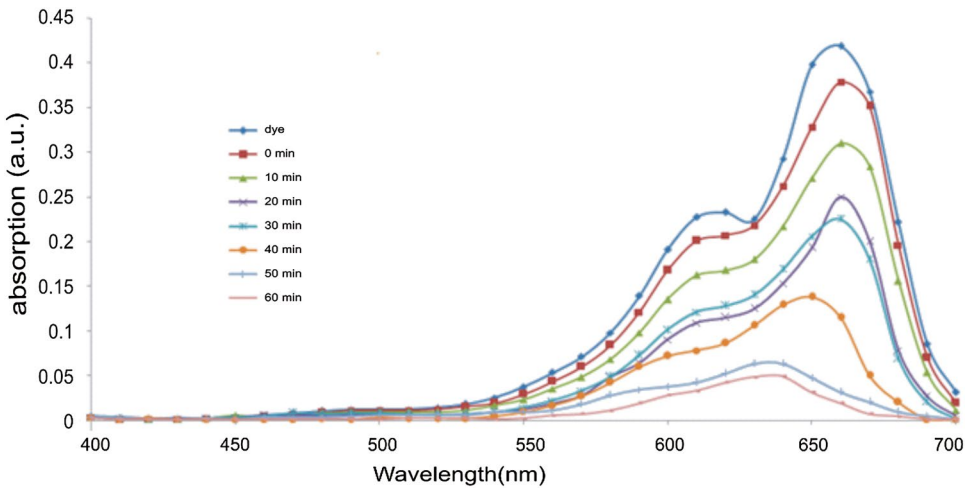

Fig. 10 Absorption spectra of MB dye solution at different time intervals of UV exposure in the presence of ZnS nanocrystals

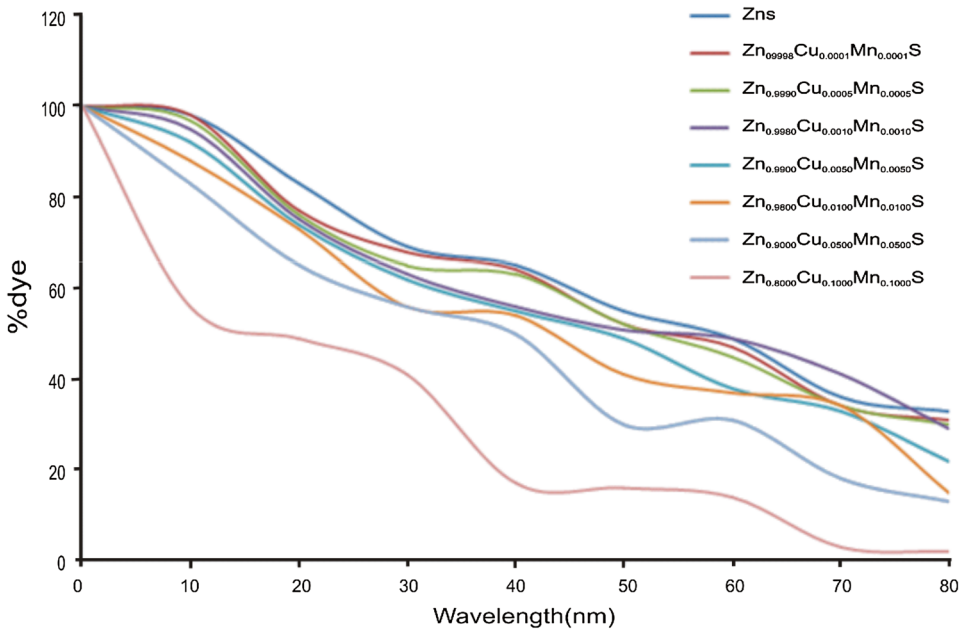

Fig. 11 Photo-catalytic degradation of MB dye by $Zn_{1-x-y}Cu_xMn_yS$ nanocrystals

4 Conclusions

Aqueous chemical co-precipitation method is an efficient facile eco-friendly synthesis technique to synthesize highly pure PVA capped $Zn_{1-x-y}Cu_xMn_yS$ $[(0 \le x \le 0.1), (0 \le y \le 0.1)]$ nanocrystals. Diffraction and electron microscope studies confirm the formation of zinc blende structured single nanocrystals having average particles size ~2–3 nm. Broad UV–Vis absorption profiles show slight blue shift with the addition of dopants. Doubly doped ZnS nanocrystals have multi-chromatic emission spectra, which strongly depends upon the doping concentration. Synthesized nanocrystals are efficient nano-photocatalysts. Host related PL emission intensity go on decreasing with addition of dopants, whereas photo-catalytic activity enhances by many folds at higher doping concentrations due to increased cross section of interfacial charge transfer.

Acknowledgements Authors are grateful to UGC, New Delhi for financial support (UGC Reference No. 20-21(12)/2012 (BSR) dated 30-03-2013).

References

1. R. Sharma, B.G. Sharma, D.P. Bisen, Photoluminescence of ZnS and ZnS: Mn nanoparticles. CSVTU Res. J. **4**(1), 25–27 (2011)
2. H.C. Warad, S.C. Ghosh, B. Hemtanon, C. Thanachayanont, J. Dutta, Luminescent nanoparticles of Mn Doped ZnS passivated with sodium hexametaphosphate. Sci. Technol. Adv. Mater. **6**, 296–301 (2005)
3. B. Bodo, R. Singh, S.C. Das, Structural and optical properties of chemically synthesized ZnS nanostructures. Int. J. Appl. Phys. Math. **2**, 4 (2012)
4. M.R. Nasrabadi, M. Behpour, A.S. Nasab, S.M. Hosseinpour-Mashkani, $ZnFe_{2-x}La_xO_4$ nanostructure: synthesis, characterization, and its magnetic properties. J. Mater. Sci. Mater. Electron. **26**, 9776–9781 (2015)
5. P. Yang, M. Lu, D. Xu, D. Yaun, G. Zhou, Synthesis and photoluminescence characteristic of doped ZnS nanoparticles. Appl. Phys. A **73**, 455–458 (2001)
6. A. Eyasu, O.P. Yadav, R.K. Bachheti, Photocatalytic degradation of methyl orange dye using Cr-doped ZnS nanoparticles under visible radiation. Int. J. Chem. Tech. Res. **5**(4), 1452–1461 (2013)
7. D. Son, D.R. Jung, J. Kim, T. Moon, C. Kim, B. Park, Synthesis and photoluminescence of Mn-doped zinc sulfide nanoparticles. Appl. Phys. Lett. **90**, 101910 (2007)
8. R. Sharma, Structural and optical characterization of ZnS nanoparticles. Int. Multidiscip. Res. J. **1**(9), 08–11 (2011)
9. D. Ayodhya, M. Venkatesham, A.S. Kumari, K.G. Mangatayaru, G. Veerabhadram, Synthesis and characterization of ZnS nanoparticles by coprecipitation method using various capping agents. IOSR J. Appl. Chem. **6**, 101–109 (2013)
10. H.V. Chung, P.T. Huy, T.T. An, Synthesis and optical properties of ZnS nanostructures. J. Korean Phys. Soc. **52**(5), 1562–1565 (2008)
11. H.S. Bhatti, N.K. Verma, S. Kumar, Lifetime measurements of doped zinc sulphide under nitrogen laser excitation. Indian J. Eng. Mater. Sci. **7**, 461–463 (2000)
12. R. Kirpal, A.K. Gupta, S.K. Mishra, R.K. Srivastava, A.C. Pandey, S.G. Prakash, Photoluminescence and photoconductivity of ZnS: Mn^{2+} nanoparticles synthesized via co-precipitation method. Spectrochimica Acta A **76**, 523–530 (2010)
13. K.T. Al-Rasoul, N.K. Abbas, Z.J. Shanan, Structural and optical characterization of Cu and Ni doped ZnS nanoparticles. Int. J. Electrochem. Sci. **8**, 5594–5604 (2013)
14. B.S.R. Devi, R. Raveendran, A.V. Vaidyan, Synthesis and characterization of Mn^{2+}-doped ZnS nanoparticles. Pramana J. Phys. **68**, 4 (2007)

15. S. Pandey, P. Verma, A.C. Pandey, *Synthesis of highly luminescent manganese doped ZnS nanophosphors*, Proceeding of ASID held at New Delhi on October 8–12, 2006 pp 259–261
16. G. Murugadoss, B. Rajamannan, V. Ramasamy, Synthesis and photoluminescence study of PVA-capped ZnS: Mn^{2+} nanoparticles. Dig. J. Nanomater. Biostruct. **5**(2), 339–345 (2010)
17. A. Murugadoss, A. Chattopadhya, Tuning photoluminescence of ZnS nanoparticles by silver. Bull. Mater. Sci. **31**(3), 533–539 (2008)
18. K. Singh, N.K. Verma, H.S. Bhatti, Photoluminescence studies of $Cd_{1-x}Zn_xS$ nanocrystals. Physica B **404**(2), 303–304 (2009)
19. M. Salavati-Niasari, F. So ofivand, A. Sobhani-Nasab, M. Shakouri-Arani, A. Yeganeh Faal, S. Bagheri, Synthesis, characterization, and morphological control of $ZnTiO_3$ nanoparticles through sol-gel processes and its photocatalyst application. Adv. Powder Technol. **27**, 2066 (2016)
20. D. Kumar, S. Bhardwaj, K. Singh, H. Bhatti, Investigation of optical and magnetic properties of synthesized $Sn_{1-x}Mn_xO_2$ nanocrystals. J. Nanosci. Nanotechnol. **17**(5), 3135–3145 (2017)